PAPER

Development of a dosimeter prototype with machine learning based 3-D dose reconstruction capabilities

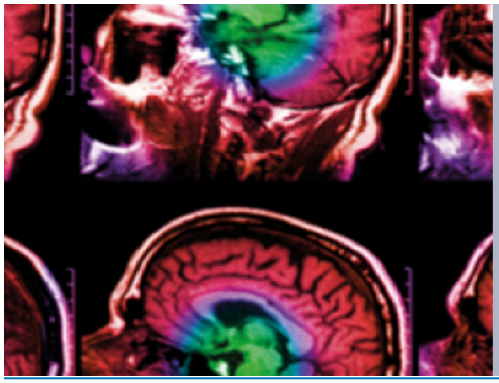

Biomedical Physics & Engineering Express

PAPER

Development of a dosimeter prototype with machine learning based 3-D dose reconstruction capabilities

G M Finneman[1], O H Eichhorn[1], N R Meskell[1], T W Caplice[1], A D Benson[1], A S Abu-Halawa[1], G L Ademoski[1], A C Clark[1], D S Gayer[1], K N Hendrickson[1], P A Debbins[2], Y Onel[2], A S Ayan[3] and U Akgun[1,*]

[1] Physics Department, Coe College, Cedar Rapids, IA, United States of America
[2] Department of Physics and Astronomy, University of Iowa, Iowa City, IA, United States of America
[3] Comprehensive Cancer Center, Ohio State University, Columbus, OH, United States of America
[*] Author to whom any correspondence should be addressed.

E-mail: uakgun@coe.edu

Keywords: dosimeters, imaging, neural network, water equivalent

RECEIVED
16 July 2021

REVISED
8 November 2021

ACCEPTED FOR PUBLICATION
12 November 2021

PUBLISHED
23 November 2021

Abstract

A 3-D dosimeter fills the need for treatment plan and delivery verification required by every modern radiation-therapy method used today. This report summarizes a proof-of-concept study to develop a water-equivalent solid 3-D dosimeter that is based on novel radiation-hard scintillating material. The active material of the prototype dosimeter is a blend of radiation-hard peroxide-cured polysiloxane plastic doped with scintillating agent P-Terphenyl and wavelength-shifter BisMSB. The prototype detector was tested with 6 MV and 10 MV x-ray beams at Ohio State University's Comprehensive Cancer Center. A 3-D dose distribution was successfully reconstructed by a neural network specifically trained for this prototype. This report summarizes the material production procedure, the material's water equivalency investigation, the design of the prototype dosimeter and its beam tests, as well as the details of the utilized machine learning approach and the reconstructed 3-D dose distributions.

1. Introduction

Radiotherapy is an ever evolving field with new methods and technologies for treatment being constantly developed. These advancements include strategies relating to intensity-modulated radiation therapy (IMRT), volumetric-modulated arc therapy (VMAT), tomography, and more recently, very-high-dose-rate (FLASH) radiotherapy [1–7]. When employing these strategies, the characterization and the measurement of correct dosage is critical, as too high of dosages can unintentionally damage healthy tissue, while too low of dosages may not achieve the intended tumoricidal effects.

The ion chamber is still the gold standard in absolute dose measurement. Various two-dimensional dosimeters have been developed to perform planar dose measurements [8, 9]. While multiple 2-D measurements could be stitched together to construct the 3-D dose distribution in a medium, a 3-D dosimeter could get the same dose distribution with a single measurement [10, 11]. Promising work has been done utilizing 3-D polymer gels [12–17], however, these gels must be read hours after irradiation due to a stabilization period similar to developing-film. Once stabilized, the optical scan used to the extract dose may also be distorted from light-reflecting and light-refracting effects which leads to error [10].

Liquid scintillators often times have good tissue-equivalence since they do not have large amounts of heavy elements relative to solids. Even though the inherent closeness to tissues would lend liquids to being ideal candidates, there are downsides. Liquid scintillators require a storage tank. This tank adds an additional layer between the radiation and the liquid. Liquid scintillators also suffer from internal reflections [18, 19]. These reflections give rise to inconsistencies in the resolved position much like scintillating gels.

Real-time measurements could also be crucial to more closely monitor the *in situ* oxygen levels and the delivered dose [6]. It has been shown that dosimeters made from scintillating materials are capable of producing real-time measurements [20–23] using devices such as plenoptic (light-field) cameras.

Scintillating dosimeters can have issues of their own. One potential issue arises if the scintillating material used to create the dosimeter is not tissue-equivalent. Tissue-equivalence helps to ensure that interactions taking place inside the dosimeter are similar to those that would take place inside of a patient [24]. However, most inorganic scintillating materials lack tissue-equivalence [6]. The material used for dosimetry must also be radiation-hard and long lasting as the dosimeters will experience high amounts of radiation over their lifetime. To that end, the effects of the scintillator's radiation damage could be mitigated with the use of tri-color LED lights [25].

Our proof-of-concept study aimed to build a solid 3-D dosimeter prototype. The prototype utilized a unique, radiation-hard, water equivalent scintillating plastic [26] as the active media. The system was tested with 6 MV and 10 MV x-ray beams. The resulting 3-D dose distributions were reconstructed by a neural network (NN) trained with 24, 000 datasets.

2. Methods

2.1. Material production

The dosimeter prototype consists of 64 scintillating bars, manufactured using Hardsil CC [26], a peroxide-cured polysiloxane, doped with primary scintillator p-Terphenyl (pTp) and wavelength-shifter Bis-MSB. This scintillating material will be referred as ScintX throughout the report.

The Hardsil CC Part A was measured into a beaker and heated to approximately 100 °C. Under moderate stirring, p-terphenyl (pTp) and Bis-MSB were added to the heated Hardsil CC Part A. The pTp and Bis-MSB were added in amounts of 1 wt.% and 0.1 wt.% respectively. Hardsil CC Part B was then added and the solution which was then stirred for approximately 15 s or until the solution became clear. The solution was then poured into a Teflon mold that had been pre-heated in a vacuum furnace at 105 °C. The vacuum chamber was evacuated and subsequently pressurized with nitrogen three times to draw out the residual air and destroy any bubbles that were formed in the bars. The bars were left to cure for 10 hours under a heating curve developed specifically for the production procedure. Figure 1 shows a few manufactured ScintX bars, before the polishing procedure, with and without UV excitation.

One of these manufactured samples was used to measure the time constant of the scintillation which was found to be 11 ns. The speed was determined by flashing a piece of ScintX with a 337 nm nitrogen laser. The resulting scintillation was collected by a PMT. The signal waveform was analyzed with a Keysight MSOX4024a oscilloscope.

2.2. Water equivalency simulation

Water equivalent materials allow for fewer conversions between humans and dosimeters. To determine quantitatively just how water equivalent ScintX is beyond the density, its mass attenuation coefficient $(\frac{m}{r})$ was calculated for an x-ray energy range of 1×10^{-3} MV. This was accomplished by using OpenGate Collaboration (Gate) [27]. A beam source with $10 \times 6^{6}\gamma$ particles was fired towards an absorber.

The absorber's material was set to ScintX then eventually water. Behind the absorber, a block of lead was placed. The lead acted as a stopping point for the penetrating particles. A particle counter was attached to the lead block. The counter was configured to only increase when a particle that had not interacted with the absorber hit the lead. The difference between a particle's initial and current energy was used to determine if it had interacted. The Mass Attenuation Coefficient was calculated using equation (1), $(\frac{m}{r})$,

$$\frac{m}{r} = -\frac{1}{dr}\ln\left(\frac{N}{N_0}\right)$$

r = Density of absorber material

d = Thickness of absorber

N = Count of non - interacting particles

N_0 = Total number of particles (1)

2.3. Detector prototype design and test beam

The detector was designed as an 8×8 array of ScintX bars each measuring $4.8 \times 80 \times 10$ mm. This array was then matched to a 64 channel, SensL 60 035, silicon photo-multiplier (SiPM) in current mode. Each SiPM pixel has a size of 5×5 mm and effective sensitivity range between 350 nm to 550 nm. The light from each individual bar was isolated through a 3D printed light guide. The light guide also served as a mounting point for the SiPM and bars. The light guide was designed using CAD and then 3D printed with white ABS plastic. The interior of the light guide was coated with Krylon Chrome Aluminum spray paint to maximize the light reflection. Each individual ScintX bar was painted with two coats of the Krylon Chrome Aluminum spray paint to prevent light leakage into adjacent bars. The generated scintillation light within the bars is directed towards the SiPMs via the light guide. Unlike the light reflected by of the walls of liquid scintillator containers, the internal reflections within the bars and light guide do not introduce error. That is because the direction of the incident light on the SiPMs does not correlate to location, instead, the channel number is used to determine the light's origin. Only the total light read by each SiPM channel is recorded.

The ends of the bars were sanded and polished to increase optical clarity which helped with light transmission. Only the ends were polished because they were where the light was exiting the bar. There was no light penetration from the sides as they were made

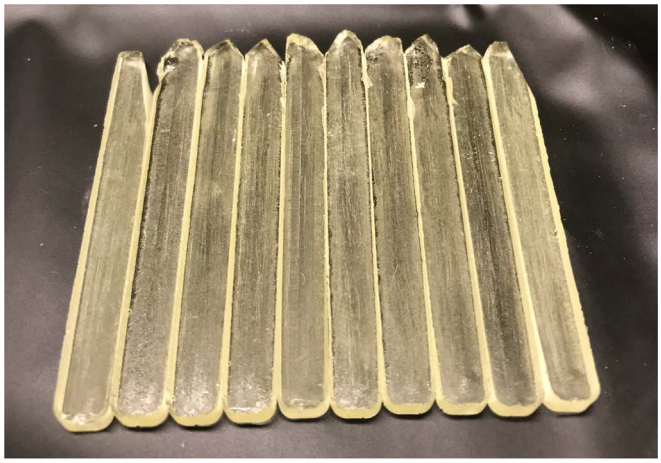

(a)

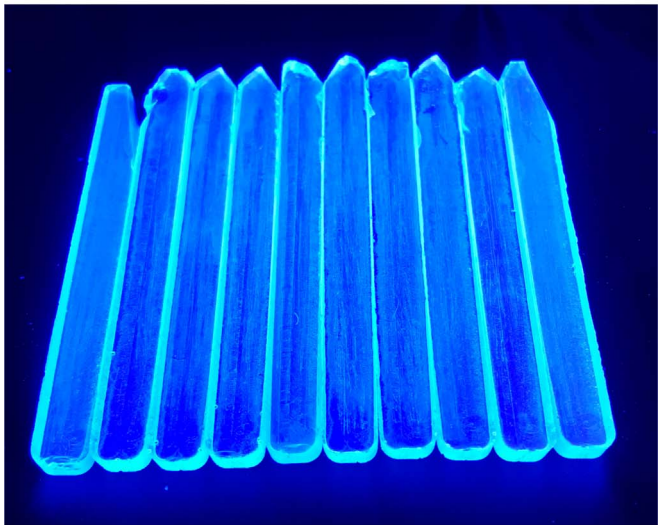

(b)

Figure 1. ScintX bars in room lighting (a) and when scintillating upon exposure to a source of UV light (b).

reflective by the paint coating. Any light that would be lost due to poor internal reflection was negligible since the bars scintillated enough to be seen with the naked eye including during data collection. The sanding also allowed the bars' dimensions to be brought within ± 1 mm of the desired 8 cm length. The polishing was carried out using a 1 μm Cerium Oxide polishing solution. The detector was then assembled and calibrated using a 12 V LED source. This calibration tested the response of each paired channel and bar with a uniform and repeatable light source, the LED. This uniformity test showed there to be less than 1% response variation between all of the channels. During the data collection in Ohio State, the detector was almost saturated thus making the small response variations between the bars negligible.

Once assembled and calibrated, the prototype was tested at the Ohio State University Comprehensive Cancer Center. The beam source utilized was a Varian TrueBeam medical linear accelerator. Two beam energies were selected: 6 MV, and 10 MV. Each energy then had multiple beam shapes fired at the detector located at the isocenter of the system: 2×2 cm, 1×3 cm, 3×1 cm, 3×3 cm, 2×4 cm, 4×2 cm, and 5×5 cm.

In order to compare the detector's performance to established baselines, dosage and penetration was collected by an Eclipse Treatment Planning System (V15.6, Varian Medical Systems) in a $40 \times 40 \times 40$ cm water bath. The source-to-surface distance was 100 cm, and the 3D dose calculation grid voxel size was $2 \times 2 \times 1.5$ mm. The calculated 3D dose distributions were exported using DICOM format.

2.4. Detector simulation

The simulations were created using Geant4 (Geant) [28] and Gate. To further aid in the automation of the simulations, JupyterHub and Jupyter-notebooks were employed [29, 30]. Via Jupyter-notebooks, Python was used as a wrapper language around the Gate macro files.

For this project two different types of detector simulations were run, one being a model of the constructed detector in real beam conditions, and a

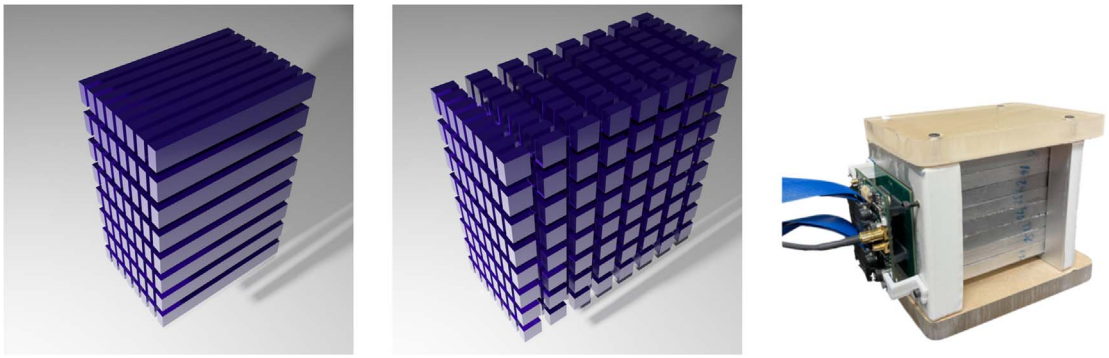

(a) (b) (c)

Figure 2. Rendered views of the simulated bar (a) and cube (b) geometries next to constructed prototype (c).

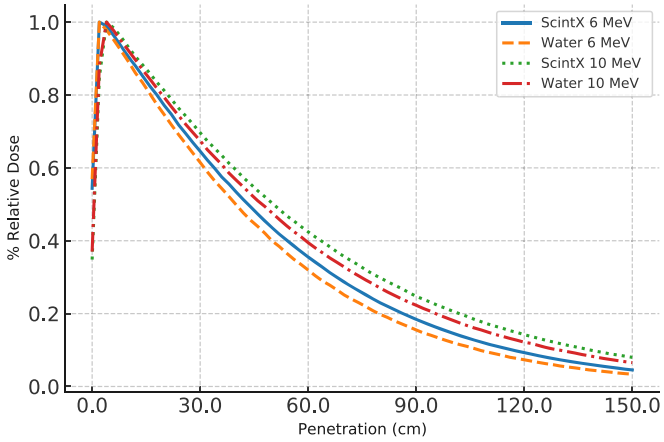

Figure 3. Simulated longitudinal energy deposition of 10^7 γ particles in water and ScintX. R^2 of 0.993 for 6 MV and 0.992 for 10 MV.

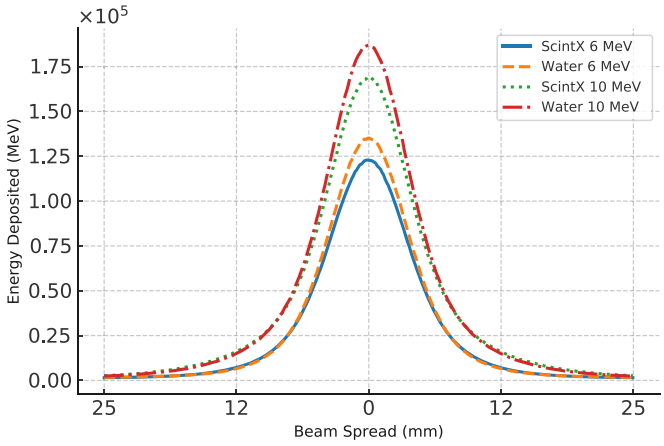

Figure 4. Simulated transverse energy deposition of 10^7 γ particles in water and ScintX. R^2 of 0.999 for 6 MV and 0.998 for 10 MV.

second, a cube version that represents the kind of output we wanted the NN to predict. Figure 2 shows these two detector geometries. The cube detector was created by breaking every bar into eight identical volumes, each measuring $4.8 \times 10 \times 10$ mm. The end result was a collection of $8 \times 8 \times 8$ cubes the same size as the 8×8 bar detector. The cube simulation served as the training data set for the machine learning.

In the simulation, the first object modeled was a single ScintX bar. It had the same dimensions as the

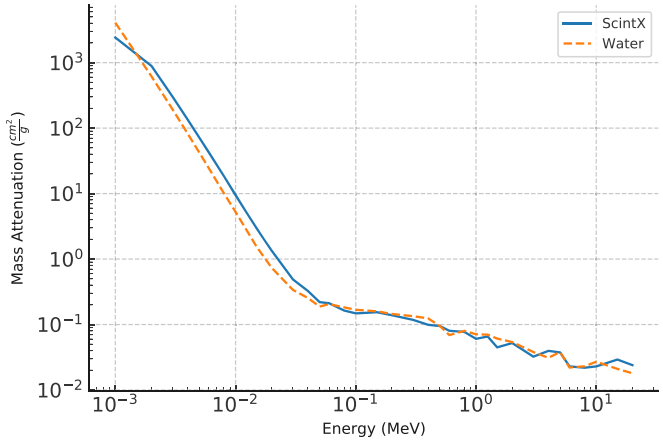

Figure 5. Simulated mass attenuation values across a range of energies for both ScintX and water. The simulated water's mass attenuation agrees strongly with values from NIST, having a MSE of 0.617 $cm^2\ g^{-1}$.

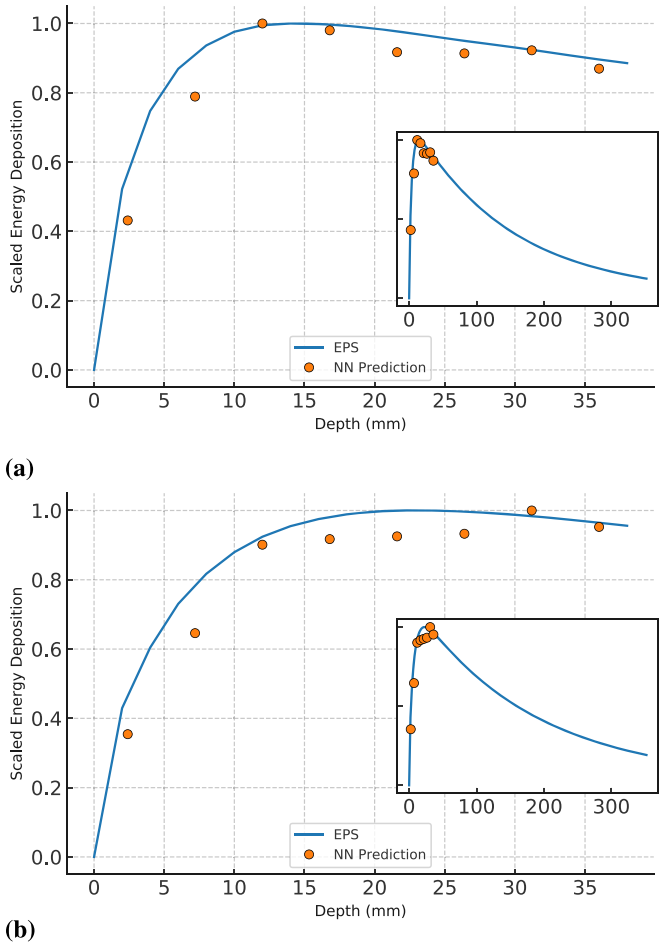

Figure 6. The graphs show the longitudinal dose distributions of the NN predictions (orange) and the dose generated by an Eclipse Treatment Planning System (blue line) with beam energies of 6 MV (a), 10 MV (b). The Beams had a cross-section of 3 × 3 cm.

ones produced in Iowa for the physical detector. This bar volume was then repeated in an 8 × 8 array leaving no gaps between adjacent copies. The material was then set to match ScintX's chemical composition. Once the geometry of the detector was created, a 10 mm cube of air was added to the world volume. Air cube served primarily as an anchoring object for the generalized particle source (gps). The simulations were performed with 1×10^6 γ particles of (1.0 ± 0.8) MV to (10.0 ± 0.8)MV in steps of 1 MV. The dimension of the beam also changed over time. Both the width and height of the beam changed from 5 mm to 50 mm in steps of 5 mm. The beam at Ohio State was used to test the prototype at 6 MV and 10 MV with

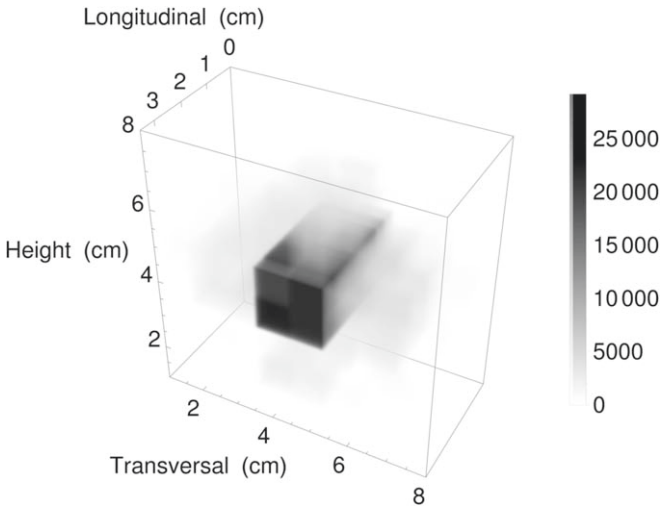

Figure 7. A NN predicted 3-dimensional dose distribution of a 6 MV 2 × 2 cm beam. The beam is traveling towards the reader.

various sizes, our simulations included those energy values and dimensions to allow comparison between simulation and real life data.

In the simulation, the distribution of energy was a Gaussian with a σ of 0.8 MV. Variations are critical to the training of NNs and limiting the training data set would have made it substantially more difficult to reconstruct the energy profiles.

Once a simulation had concluded, the energy deposition in each volume (bar or cube depending) was written to a text file. Each file has the unique set of energy, width, height, and rotation angle values encoded in the name to prevent loss of data. For processing purposes the millions of small edep interactions were summed up on a volume by volume basis to yield either 512 or 64 different sums depending on whether the file corresponds to a bar simulation or cube simulation.

Our detector is intended to be shot with radiation then rotated 90° and irradiated again. The simulation takes this into account by having the detector rotated in the world volume. For every combination of beam size and energy, the model was rotated 360° in steps of 15°. In total, there were 24, 000 bar and cube simulation pairs. Each pair serves as one training data point for the NN.

2.5. Neural net development

The neural network (NN) was programmed using Julia and a package called FLUX [31, 32]. This was again all done in a Jupyter-notebook. The NN was given training data created in the Gate simulations. The composition of the NN included two convolutional layers, two dense layers, and one dropout layer.

The NN used two convolutional layers, both with 2 × 2 filters as the first and second layers in the model. The first convolutional layer expanded the two bar-data channels into eight channels. These eight channels no longer have physical representations, but instead represent patterns the NN recognized while scanning the data with the 2 × 2 filter. The second conv layer then took those resulting eight channels and expanded them into sixteen channels. After this process, a drop-out layer was inserted. This layer randomly selects 5% of its neurons and resets their learned influence to zero. This helps prevent memorization. Lastly, the NN has two dense layers. These are fully-connected layers and help to process the ouput of the convolutions.

The dense layers in the NN have sizes 1600 × 900 and 900 × 512 neurons respectively. The 512 points of data output by the last layer was reshaped into an 8 × 8 × 8 array. The reshaping was done to more directly store the data in a format representative of the cube detector. The end result is a NN that trains on two 8 × 8 sets of bar data and outputs a single 8 × 8 × 8 array of cube data.

The NN utilized the standard activation function RELU (rectified linear unit). RELU will pass along any positive value directly without changing it, and will convert any negative value to 0. Testing of other activation functions decreased the NN's performance. The optimizer chosen for our NN was ADAM as it is predictable and the industry standard for stochastic gradient descent.

The largest problem facing the NN is over-fitting. Over-fitting occurs when a NN learns to directly recreate outputs from certain inputs rather than learning a general recreation algorithm for any input. To prevent over training from becoming a problem, 16% of the input data was held aside until the validation phase of training. After each complete training cycle, the validation data was run through the NN. If the accuracy of the validation outputs became worse according the an R^2 test, training was halted via early-stopping. In addition to early stopping, the dropout layer early on in the NN structure combats the progress of over training.

3. Results

3.1. Water equivalency

The density of ScintX was measured to be 0.96 g cm^{-3} and from this, the electron density and Z/A ratio were calculated to be 3.000×10^{23} e cm^{-3} and 0.5189 respectively. These compare well to water, which has an electron density and a Z/A ratio of 3.343×10^{23} e cm^{-3} and 0.5551 respectively. These are also similar to other scintillating materials that aim to be water-equivalent for dosimeter use [24].

The longitudinal and transverse x-ray energy depositions in ScintX and water were compared via Gate simulations where 10^7 γ were directed to a volume filled with ScintX (and water). Figure 3 shows the longitudinal dose distributions within ScintX are in agreement with those of water with R^2 of 0.993 for 6 MV and 0.992 for 10 MV. The transverse energy distributions comparison between water and ScintX, shown in figure 4, yields R^2 of 0.999 for 6 MV and 0.998 for 10 MV.

The Gate simulations were also used to calculate the Mass Attenuation Coefficients (M.A.C) for ScintX and water. Figure 5 shows the mean square error between the water and ScintX M.A.C. values is 0.617 cm^2 g^{-1} over the range from 10×10^{-3} MV to 10 MV.

3.2. Reconstructed dose distributions

The NN was able to predict energy depositions from Geant4 simulated data it had never seen before with an R^2 accuracy of up to 0.925. This was achieved after the NN had trained on 20, 000 sets of data. This number is not the total number of simulation pairs produced because 20% were held aside for validating the training.

The data recorded by the prototype at Ohio State University was also run through the NN. The total energy predicted by the NN at each depth and width was calculated and compared to a percent depth dose generated by the Eclipse Treatment Planning System. The comparison showed that the detector and NN were able to successfully reproduce results similar to the percent depth dose.

In figure 6 comparison plots, the maximum value of each of the data sets was scaled to match. The Eclipse Treatment Planning System uses the highest energy deposited voxel at each depth, meanwhile the prototype's NN predicted energy deposition at each layer is summed and scaled to obtain the longitudinal as well as the transverse distributions. The longitudinal profiles reported in figure 6 are representative of seven different beam shapes. The transverse distribution reconstructions were not as successful mainly due to the larger 1 cm resolution along that direction of the detector.

4. Conclusion

The purpose of this study was to develop a fast and accurate 3-D dosimeter that can be effectively and repeatedly used for real-time measurements in radiotherapy. This study introduced a novel, water-equivalent, radiation-hard, fast, scintillating plastic (ScintX). This material was used to build a proof-of-concept prototype detector. Its performance was tested in a clinical radiotheraphy 6 MV and 10 MV x-ray beams at The Ohio State University. A NN was designed and trained to predict the 3-D dose distribution based on the collected data as shown in figure 7. The predicted 3-D dose distribution clearly shows the beam profile. The halo around the beam is likely an artifact of collecting data in two perpendicular detector orientations. Since the thickness of the detector is 38.4 mm, the entire distribution for energy deposition in water is not seen due to over-penetration. This phenomenon is corroborated by figure 6 which shows the energy deposition in the detector region in relation to a larger water region.

The results show, once trained, the NN can process the data quickly and generate a 3-D dose reconstruction. The predicted dose distribution within the detector was compared to depth dose calculations generated by the Eclipse Treatment Planning System. The data shows that the device can successfully predict the longitudinal dose distribution within the first 35 mm of depth.

Future studies for this approach will focus on building a detector with a larger volume and higher spatial resolution. More research on the material is required to reduce the dimensions of the individual bars in order to increase the resolution of the device, which will also reduce light loss from the light guide. The accuracy of the NN predictions can also be improved with ever improving machine learning algorithms, and yield higher resolution 3-D dose distributions. This proof-of-concept study yields encouraging results that can be improved and applied to various dosimetric applications. Considering the fast time constant of ScintX (<15 ns), it may be suitable for FLASH radiotherapy, which may deposit up to 1000 Gy in 500 ms [33, 34].

Acknowledgments

This work was funded by Coe College, NSF-RUI (1746230), NSF-REU (1659581, 1950337), R.J. McElroy Trust Student/Faculty Research Fund.

Data availability statement

The data that support the findings of this study are available upon reasonable request from the authors.

ORCID iDs

G M Finneman https://orcid.org/0000-0003-4048-2027
A S Ayan https://orcid.org/0000-0002-8554-5426
U Akgun https://orcid.org/https://orcid.org/0000-0002-9850-4164

References

[1] Spirou S V and Chui C S 1994 Generation of arbitrary intensity profiles by dynamic jaws or multileaf collimators *Med. Phys.* **21** 1031–41
[2] Stein J *et al* 1994 Dynamic X-ray compensation for conformal radiotherapy by means of multi-leaf collimation *Radiother. Oncol.* **32** 163–73
[3] Yu C X 1995 Intensity-modulated arc therapy with dynamic multileaf collimation: An alternative to tomotherapy *Phys. Med. Biol.* **40** 1435–49
[4] Otto K 2008 Volumetric modulated arc therapy: IMRT in a single gantry arc *Med. Phys.* **35** 310–7 (https://aapm.onlinelibrary.wiley.com/doi/10.1118/1.2818738)
[5] Kinsella T and Deasy J O 1993 Tomotherapy: A new concept for the delivery of dynamic conformal radiotherapy *Med. Phys.* **20** 1709–19 (https://aapm.onlinelibrary.wiley.com/doi/10.1118/1.596958)
[6] Ashraf M R *et al* 2006 *Dosimetry for FLASH Radiotherapy: A Review of Tools and the Role of Radioluminescence and Cherenkov Emission* arXiv: 2006.03755
[7] Rilling M *et al* 2020 Tomographic-based 3D scintillation dosimetry using a three-view plenoptic imaging system *Med. Phys.* **47** 3636–46
[8] Pönisch F *et al* 2009 Liquid scintillator for 2D dosimetry for high-energy photon beams *Med. Phys.* **36** 1478–85
[9] Dempsey J F *et al* 2000 Validation of a precision rediochromic film dosimetry system for quantitative two-dimensional imaging of acute exposure dose distributions *Med. Phys.* **27** 2462–75
[10] Doran S J 2009 The history and principles of chemical dosimetry for 3-D radiation fields: Gels, polymers and plastics *Appl. Radiat. Isot.* **67** 393–8
[11] Low D A *et al* 2011 Dosimetry tools and techniques for IMRT *Med. Phys.* **38** 1313–38
[12] Khezerloo D *et al* 2017 PRESAGE® as a solid 3-D radiation dosimeter: A review article *Radiation Physics and Chemistry* **141** 88–97
[13] Adamovics J and Maryanski M J 2006 Characterisation of PRESAGE™: A new 3-D radiochromic solid polymer dosemeter for ionising radiation *Radiat. Prot. Dosimetry* **120** 107–12
[14] Adamovics J and Maryanski M J 2004 A new approach to radiochromic three-dimensional dosimetry-polyurethane *J. Phys. Conf. Ser.* **3** 172–5
[15] Adamson J *et al* 2014 On the feasibility of polyurethane based 3D dosimeters with optical CT for dosimetric verification of low energy photon brachytherapy seeds *Med. Phys.* **41** 7
[16] Crescenti R A *et al* 2007 Introducing gel dosimetry in a clinical environment: Customization of polymer gel composition and magnetic resonance imaging parameters used for 3D dose verifications in radiosurgery and intensity modulated radiotherapy *Med. Phys.* **34** 1286–97
[17] Gore J C *et al* 1996 Radiation dose distributions in three dimensions from tomographic optical density scanning of polymer gels: I. Development of an optical scanner *Phys. Med. Biol.* **41** 2695–704
[18] Archambault L *et al* 2012 Verification of proton range, position, and intensity in IMPT with a 3D liquid scintillator detector system *Med. Phys.* **39** 1239–46
[19] Beddar A S 2006 Water equivalent plastic scintillation detectors in radiation therapy *Radiat. Prot. Dosimetry* **120** 1–6
[20] Darne C *et al* 2019 3D Scintillator Detector System for Proton Scanning Beam Therapy *Int. J. Radiat. Oncol.* **105** S89–90
[21] Darne C D *et al* 2017 Performance characterization of a 3D liquid scintillation detector for discrete spot scanning proton beam systems *Phys. Med. Biol.* **62** 5652–67
[22] Vigdor S E *et al* 2017 A gas scintillator detector for 2D dose profile monitoring in pencil beam scanning and pulsed beam proton radiotherapy treatments *Phys. Med. Biol.* **62** 4946–69
[23] Goulet M *et al* 2014 Novel, full 3D scintillation dosimetry using a static plenoptic camera *Med. Phys.* **41** 082101
[24] Beddar A S 2006 Plastic scintillation dosimetry and its application to radiotherapy *Radiat. Meas.* **41** S124–33
[25] Wetzel J *et al* 2017 Using LEDs to stimulate the recovery of radiation damage to plastic scintillators *Nucl. Instruments Methods Phys. Res. Sect. B Beam Interact. with Mater. Atoms* **395** 13–6
[26] Akgun Ugur O Y *et al* 2020 Apparatus, system, and method for radiation hardened plastic and flexible elastomer scintillator *Apparatus, system, and method for radiation hardened plastic and flexible elastomer scintillator* US20200264323A1(https://patents.google.com/patent/US20200264323A1/en?inventor=Ugur+Akgun&oq=Ugur+Akgun)
[27] Sarrut D *et al* 2014 A review of the use and potential of the GATE Monte Carlo simulation code for radiation therapy and dosimetry applications *Med. Phys.* **41** 64301–2
[28] Agostinelli S *et al* 2003 GEANT4—A simulation toolkit *Nucl. Instruments Methods Phys. Res. Sect. A Accel. Spectrometers, Detect. Assoc. Equip.* **506** 250–303
[29] Kluyver T *et al* 2016 Jupyter Notebooks—a publishing format for reproducible computational workflows *Paper presented at the: Position. In Position. Power Acad. Publ. Play. Agents Agendas* ed F Loizides and B Schmidt (Amsterdam, Netherlands: IOS Press)
[30] Van Rossum G and Drake F L 2009 Python 3 Reference Manual *Python 3 Reference Manual* ed Guido Van Rossum and Fred Drake (Scotts Valley, CA: CreateSpace) Scotts Valley, CACreateSpace
[31] Bezanson J *et al* 2017 Julia: A fresh approach to numerical computing *SIAM Rev.* **59** 65–98
[32] Innes M *et al* (2018) Fashionable Modelling with Flux *CoRR* abs/1811.0
[33] Favaudon V *et al* 2014 Ultrahigh dose-rate FLASH irradiation increases the differential response between normal and tumor tissue in mice *Sci. Transl. Med.* **6** 245
[34] Montay-Gruel P *et al* 2021 Hypofractionated FLASH-RT as an Effective Treatment against Glioblastoma that Reduces Neurocognitive Side Effects in Mice *Clin. Cancer Res.* **27** 775–84